On POD analysis of PIV measurements applied to mixing in a stirred vessel with a shear thinning fluid

A. Liné [a,b,c,*], J.-C. Gabelle [a,b,c,d,e], J. Morchain [a,b,c], D. Anne-Archard [f], F. Augier [e]

[a] *Université de Toulouse, INSA, LISBP, 135 Avenue de Rangueil, F-31077 Toulouse, France*
[b] *INRA UMR792 Ingénierie des Systèmes Biologiques et des Procédés, Toulouse, France*
[c] *CNRS, UMR5504, F-31400 Toulouse, France*
[d] *ADEME French Environment and Energy Management Agency, 20 avenue du Grésillé, BP 90406, 49004 Angers Cedex 01, France*
[e] *IFP Energies nouvelles, Rond-point de l'échangeur de Solaize, BP3, 69360 Solaize, France*
[f] *Université de Toulouse, INPT, UPS, IMFT, Allée C. Soula, F-31400 Toulouse, France*

ABSTRACT

P.O.D. technique is applied to 2D P.I.V. data in the field of hydrodynamics in a mixing tank with a Rushton turbine and a shear thinning fluid. Classical eigen-value spectrum is presented and phase portrait of P.O.D. coefficients are plotted and analyzed in terms of trailing vortices. A spectrum of dissipation rate of kinetic energy is introduced and discussed. Length scales associated to each P.O.D. modes are proposed.

Keywords: Mixing; Particle image velocimetry; Proper orthogonal decomposition; Eigenvalue spectrum; Dissipation rate; Stirred tank

1.   Introduction

Advanced experimental techniques such as particle image velocimetry (P.I.V.) are available nowadays, and they generate a huge amount of data, in terms of instantaneous velocity fields (in a plane as far as 2D P.I.V. is concerned). Indeed, advanced data processing tools are required to extract more and more information from this source of experimental data. Proper orthogonal decomposition (P.O.D.) or Karhunen–Loeve method that is known to be efficient to isolate coherent structures from a series of instantaneous velocity fields (Berkooz et al., 1993) will be used in this paper. P.O.D. is a modal decomposition of instantaneous velocity fields, the modes being orthogonal to each others. It can be expressed as:

$$\vec{V_k}(x, y, z, t) = \sum_{I=1}^{N} \overrightarrow{V_k^{(I)}}(x, y, z, t) = \sum_{I=1}^{N} a_k^{(I)}(t) \overrightarrow{\Phi^{(I)}}(x, y, z) \tag{1}$$

where $\vec{V_k}$ is the kth instantaneous event of velocity field measurement and $\overrightarrow{V_k^{(I)}}$ is the Ith component of the P.O.D.

decomposition. For each mode I, the P.O.D. method generates temporal coefficients $a_k^{(I)}$ and spatial modes $\overrightarrow{\Phi^{(I)}}$. $a_k^{(I)}(t)$ is an instantaneous (k) or temporal (t) scalar (called P.O.D. coefficient of P.O.D. mode I); it is independent of space. $\overrightarrow{\Phi^{(I)}}(x, y, z)$ is a spatial eigenfunction of mode I and it is independent of time (or instantaneous event k). Modes can be derived from the Fredholm eigenvalue integral equation, adapted by Sirovich (1987) as:

$$\iint_{\Omega} R(x, y, z, x', y', z') \overrightarrow{\Phi^{(I)}}(x', y', z') \, dx' \, dy' \, dz' = \lambda^{(I)} \overrightarrow{\Phi^{(I)}}(x, y, z) \tag{2}$$

where R is the cross-correlation tensor and $\lambda^{(I)}$ is the eigenvalues. Following this approach, the eigenvalues are expressed in m^5/s^2 in a full 3D analysis. Indeed, one can point out that the dimension corresponds to a kinetic energy (m^2/s^2) times a volume ($dx\,dy\,dz$). In 2D PIV problem, the eigenvalues are expressed in m^4/s^2, corresponding to a kinetic energy (m^2/s^2) times a surface ($dx\,dz$). Usually eigenvalue sequences are ranked in decreasing order. Clearly, this ordering of eigenvalues ensures that the first P.O.D. modes are the most energetic.

* *Corresponding author at*: Université de Toulouse, INSA, LISBP, 135 Avenue de Rangueil, F-31077 Toulouse, France. Tel.: +33 561559786; fax: +33 561559760.
E-mail address: alain.line@insa-toulouse.fr (A. Liné).

Given its eigenvalue, $\lambda^{(1)}$ and its eigenfunction $\overrightarrow{\Phi^{(I)}}(x, y, z)$, it is possible to reconstruct the velocity field associated to the mode 1 $(\overrightarrow{V_k^{(1)}}(x, y, z, t))$ which will be confirmed to represent the mean flow. Considering modes 2 and 3, Oudheusden et al. (2005) have shown that, when their P.O.D. eigenvalues are close to each other, the POD modes are coupled: usually, they correspond to orthogonal components of a periodic process (coherent structures induced by the blades of the impeller). Higher modes correspond to lower eigenvalues that are associated to smaller scale structures. Knight and Sirovich (1990) have shown that the eigenvalue spectrum (plot of eigenvalues versus mode number I) exhibit $I^{-11/9}$ trend in the inertial subrange of turbulence. This trend was confirmed by De Angelis et al. (2003) and Hoisiadas et al. (2005) (among others). The analysis of the different modes will be addressed in this paper, in the field of mixing in a stirred tank with a Rushton turbine and a shear thinning fluid. In addition, a spectrum of dissipation rate of kinetic energy associated to each mode I, similar to the spectrum of eigenvalues, will be presented and discussed. Characteristic length scales (wave length) associated to each mode will be also proposed.

As highlighted by many authors, P.O.D. eigenfunctions present flow-field-like structures and their analysis must be driven with care. However, the significance of P.O.D. modes can become clearer by the detailed analysis of P.O.D. coefficients $a_k^{(I)}$. Some relation between two modes I and J can be tracked down by plotting the two coefficients series $[a_k^{(I)}, a_k^{(J)}], k = 1, N$ in the $(a^{(I)}, a^{(J)})$ plane. Such a plot is called a 2D projection of the phase portrait. Hydrodynamic coherent structures can be revealed when characteristic patterns appear in this plane, such as circle, ellipse or Lissajous figures that can be associated to periodic or intermittent structures. In particular, circular shapes can suggest cyclic variations of modes I and J related to vortices or coherent structures. In this case, $(a^{(I)}, a^{(J)})$ series can be modeled as sine–cosine functions with same period. Such phase portraits will be plotted in this paper in order to emphasize the coupling between modes 2 and 3, associated to trailing vortices generated by the blades of the impeller.

P.O.D. was applied to hydrodynamics in mixing tank by Moreau and Liné (2006), Doulgerakis (2010), and Gabelle et al. (2013). Snapshot P.O.D. studies were reviewed by Tabib and Joshi (2008) in the field of Chemical Engineering. The goal of this paper is to contribute to extract information from 2D P.I.V. data by P.O.D. technique in the field of mixing. Classical P.O.D. data processing is performed in terms of eigenvalue problem, spectrum of eigenvalues and phase portrait analysis. New data processing is proposed in terms of dissipation rates and wavelengths associated to each mode I.

2. Materials and methods

2.1. Mixing tank

2D-P.I.V. measurements were performed in a 70 L stirred tank equipped with four equally spaced baffles. A Rushton turbine (D/T = 0.33) was used. The vessel was standard ($T = 0.45$ m); the impeller clearance was $C = T/3$. More information about the mixing tank dimensions is provided in Gabelle et al. (2013).
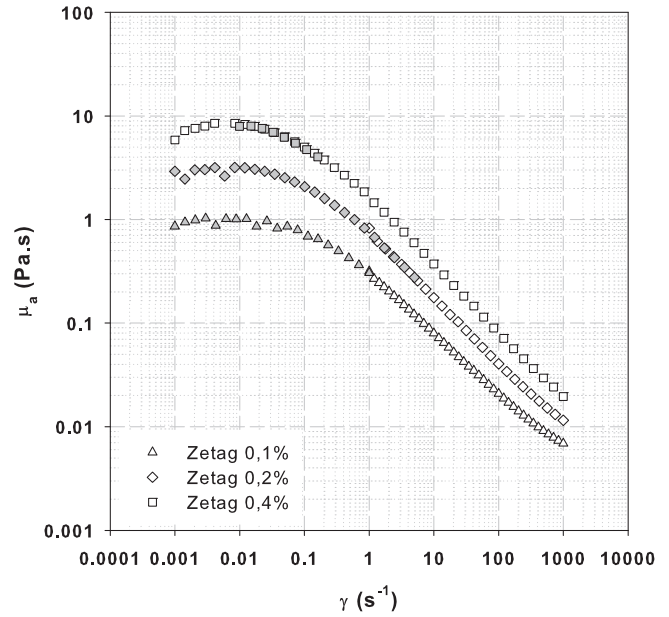

Fig. 1 – Apparent viscosity of Zetag7587 solutions versus shear rate.

2.2. P.I.V. system

The P.I.V. system used in this study consisted of a laser and an image acquisition system provided by LaVision (LaVision GmbH, Goettingen, Germany). The system included a laser Nd-Yag (Quantel, 10 Hz, 200 × 2 mJ), a synchronization system and a charge-coupled-device (CCD) camera (Imager Intense, 12 bits, 1376 × 1040 pixels). Fast Fourier transform (FFT) cross correlation was used to interrogate the two images, which were divided into interrogation area (32 × 32 or 16 × 16 pixels). For all experiments, 500–700 image pairs were recorded and statistical convergence of the velocity was checked. In order to study the influence of spatial resolution on the vicinity of the impeller, two spatial resolutions Δx (0.7–1 mm) were tested. The delay between each frame in an image pair was chosen in relation to the impeller rotational speed. Four zones in the vessel were investigated: one in the impeller steam, two above and one below. POD was only carried out for the image at the impeller level.

2.3. Working fluid

The shear thinning fluid Zetag7587 (BASF, Ludvigshafen, Germany) was used. It offers good transparency even at high concentration (0.4%). Rheological measurements were carried out using a Haake Mars III rheometer (ThermoHaake, Germany). Flow curves of Zetag7587 solutions are presented in Fig. 1 for shear rates ranging from 0.001 to 1000 s^{-1}. Rheological data can be fitted to the model of Ostwald de Waele (power law) according to:

$$\mu_a = K|\dot{\gamma}|^{n-1} \qquad (3)$$

with K the fluid consistency factor and n the flow index. The rheological parameters are reported in Table 1. Zetag7587 is known to be visco-elastic (Escudier and Smith, 2001). However, the choice of Zetag7587 at a high concentration 0.4% was made because at high concentration the viscosity is high; it is thus easier to measure turbulent flow characteristics close to the impeller, the turbulent microscales being larger at relatively

Table 1 – Rheological parameters fitted to the power law equation.

Fluid	n	K (Pa s^n)	Shear rate range (s^{-1})
Zetag7587 0.1%	0.422	0.30	1–350
Zetag7587 0.2%	0.376	0.74	1–600
Zetag7587 0.4%	0.349	1.65	1–1000

low Reynolds number and the spatial resolution of PIV measurement needed to catch the physics being larger.

2.4. Experimental conditions

The impeller speed N is 205 rpm. The global shear rate $\dot{\gamma}_{MO}$ is estimated from Metzner–Otto correlation:

$$\dot{\gamma}_{MO} = k_S N \tag{4}$$

where the constant k_S depends on the impeller type ($k_S = 11.5$ for a Rushton turbine). The shear rate is thus equal to $40\,\text{s}^{-1}$. Given the rheological law of the shear thinning fluid, the apparent viscosity is 0.15 Pa s. The Reynolds number is thus equal to 530, corresponding to the transition region between laminar and turbulent regime. The volume averaged value of the dissipation rate of kinetic energy $\langle \varepsilon \rangle$ can be estimated; it is equal to $\langle \varepsilon \rangle = 0.2$ m^2/s^3 or W/kg. The associated value of global shear rate is $\langle \gamma \rangle = 37\,\text{s}^{-1}$. Indeed, the flow is turbulent close to the impeller and less and less turbulent far from it. The P.I.V. data were acquired in a domain close to the impeller tip (6 cm × 6 cm), ensuring turbulent flow conditions as it will be shown in the results presentation and discussion.

3. Data processing

Proper orthogonal decomposition (P.O.D.) is a linear procedure, which decomposes a set of instantaneous velocity fields into a modal base (see Section 3.1). We propose in this work to investigate P.O.D. in terms of reconstruction of instantaneous velocity fields in a mixing tank. This methodology allows separating the organized and the turbulent motions without the necessity to collect angular phased data (Moreau and Liné, 2006). POD is carried out using snapshot method with all the sets of instantaneous velocity fields directly issued from the measurements. The result is then an orthonormal basis of eigenfunctions and associated eigenvalues. The instantaneous velocity field can be projected on each POD eigenfunction. From these projections it is possible to get P.O.D. coefficients and to reconstruct the velocity field (see Section 3.2). Dissipation rate of kinetic energy can be estimated from the 2D velocity field (Section 3.3). Finally, characteristic length scales may also be determined from the PIV experiments.

3.1. Snapshot method

P.I.V. measurements are performed in the (x,z) plane, on a regular mesh with L rows and C columns, leading to $NP = L\,C$ points per plane. Each instantaneous velocity field measurement constitutes a snapshot of the flow. The statistical analysis is performed on N snapshots taken in the same plane (P.I.V. data).

The number of grid points being LC, one obtains the matrix of instantaneous velocity vector data as:

$$\overrightarrow{V_k^{(1)}}x = \begin{bmatrix} \overrightarrow{V_k}(x_1, z_1) & \overrightarrow{V_k}(x_1, z_2) & \overrightarrow{V_k}(x_1, z_C) \\ \overrightarrow{V_k}(x_2, z_1) & \overrightarrow{V_k}(x_2, z_2) & \overrightarrow{V_k}(x_2, z_C) \\ & & \\ \overrightarrow{V_k}(x_L, z_1) & \overrightarrow{V_k}(x_L, z_2) & \overrightarrow{V_k}(x_L, z_C) \end{bmatrix} \tag{5}$$

where k is the index of the instantaneous event ($k = 1, N$). This matrix of vectors can be reshaped to build a vector $\overrightarrow{V_k}$ with $2LC$ rows as follows:

$$\overrightarrow{V_k} = \begin{bmatrix} u_k(x_1, z_1) \\ u_k(x_2, z_1) \\ \\ u_k(x_L, z_C) \\ w_k(x_1, z_1) \\ w_k(x_2, z_1) \\ \\ w_k(x_L, z_C) \end{bmatrix} \tag{6}$$

The snapshot method adopted in this eigenvalue problem was proposed by Sirovich (1987). This method is based on the snapshot matrix M corresponding to the N instantaneous velocity fields. The matrix M can be expressed as

$$M = \begin{bmatrix} u_1(x_1, z_1) & u_2(x_1, z_1) & \dots & u_N(x_1, z_1) \\ u_1(x_2, z_1) & u_2(x_2, z_1) & \dots & u_N(x_2, z_1) \\ & & \dots & \\ u_1(x_L, z_C) & u_2(x_L, z_C) & \dots & u_N(x_L, z_C) \\ w_1(x_1, z_1) & w_2(x_1, z_1) & \dots & w_N(x_1, z_1) \\ w_1(x_2, z_1) & w_2(x_2, z_1) & \dots & w_N(x_2, z_1) \\ & & \dots & \\ w_1(x_L, z_C) & w_2(x_L, z_C) & \dots & w_N(x_L, z_C) \end{bmatrix} \tag{7}$$

The matrix M has $2LC$ rows and N columns, each column of the matrix M representing the kth event of the instantaneous velocity field. The auto-covariance tensor R can be derived as:

$$R = \frac{1}{N}M.M^T = \begin{bmatrix} \overline{u^2(x_1, z_1)} & & \\ & \dots & \\ & & \overline{w^2(x_L, z_C)} \end{bmatrix} \tag{8}$$

The Fredholm integral eigenvalue problem is represented in the 2D domain Ω of measurement by:

$$\iint_\Omega R(x, z, x', z') \overrightarrow{\Phi^{(l)}}(x', z')\,dx'dz' = \lambda^{(l)}\overrightarrow{\Phi^{(l)}}(x, z) \tag{9}$$

where $\lambda^{(l)}$ is the lth eigenvalue and $\overrightarrow{\Phi^{(l)}}x(x, z)$ is the lth associated eigenfunction. The correlation tensor can be expressed in the orthonormal basis as a diagonal matrix. The eigenvalues of R, $\lambda_R^{(l)}$, are expressed in m^2/s^2 and are defined as: $\lambda_R^{(l)} = \lambda^{(l)}/(dx\,dz)$.

The dimension of $M.M^T$ matrix is $(2LC)^2$ whereas the dimension of $M^T.M$ matrix is N^2. The eigenfunctions of $M.M^T$

are $\overrightarrow{\Phi^{(I)}}(x, z)$; they can be simply related to the eigenvalues of $M^T.M$, noted $\overrightarrow{\Phi'^{(I)}}(x, z)$, as:

$$\overrightarrow{\Phi'^{(I)}}(x, z) = M^T \overrightarrow{\Phi^{(I)}}(x, z) \quad \text{or} \quad \overrightarrow{\Phi^{(I)}}(x, z) = M\overrightarrow{\Phi'^{(I)}}(x, z) \tag{10}$$

This must be kept in mind in order to save computing time since $M.M^T$ and $M^T.M$ have identical eigenvalues, but may have significantly different sizes if $N^2 \ll (2LC)^2$. In addition, the spatial modes constitute an orthonormal basis, thus:

$$\overrightarrow{\Phi^{(I)}}.\overrightarrow{\Phi^{(J)}} = \delta_{IJ} \tag{11}$$

3.2. Modal decomposition of the velocity field

Each instantaneous velocity field or snapshot of the flow can be expanded in a series of P.O.D. modes. The P.O.D. coefficients $a_k^{(I)}$ are obtained by projecting each instantaneous velocity field on the Ith eigenfunction $\overrightarrow{\Phi^{(I)}}$:

$$a_k^{(I)} = \overrightarrow{V_k}.\overrightarrow{\Phi^{(I)}} \tag{12}$$

The Ith velocity vector $\overrightarrow{V_k^{(I)}}$ corresponding to the Ith decomposition is given by:

$$\overrightarrow{V_k^{(I)}} = a_k^{(I)}\overrightarrow{\Phi^{(I)}} \tag{13}$$

One can thus reconstruct each instantaneous velocity field given by Eq. (1). One can easily derive:

$$\frac{1}{N}\sum_{k=1}^{N}a_k^{(I)}a_k^{(J)} = \lambda_R^{(I)}\delta_{IJ} \tag{14}$$

This relation shows that each mode makes an independent contribution to the total kinetic energy.

3.3. Modal decomposition of the dissipation rate of kinetic energy

The rate of viscous dissipation of kinetic energy is defined as:

$$\varepsilon = 2\nu_a \overline{S:S} \tag{15}$$

where ν_a is the apparent viscosity of the fluid and S is the strain rate (or stretching) tensor, defined as:

$$\lambda^{(I)} \propto \kappa^{-11/3} \tag{16}$$

Considering the decomposition of the velocity field in the sum of Ith components, one can associate to each Ith component of the velocity $V_{i,k}^{(I)}$ a component $S_{ij,k}^{(I)}$ of the strain rate tensor:

$$S_{ij,k}^{(I)} = \frac{a_k^{(I)}}{2} \cdot \left(\frac{\partial \Phi_i^{(I)}}{\partial x_j} + \frac{\partial \Phi_j^{(I)}}{\partial x_i}\right) \tag{17}$$

Accounting for Eqs. (11) and (14), one can thus derive the Ith component of the rate of viscous dissipation of kinetic energy:

$$\varepsilon^{(I)} = \nu_a(\dot{\gamma})\frac{\lambda_R^{(I)}}{2}\sum_{i=1}^{3}\sum_{j=1}^{3}\left(\frac{\partial \Phi_i^{(I)}}{\partial x_j} + \frac{\partial \Phi_j^{(I)}}{\partial x_i}\right)^2 \tag{18}$$

It is interesting to realize that the total dissipation rate of kinetic energy is the sum of the Ith component of the rate of viscous dissipation of kinetic energy: $\varepsilon(x, z, t) = \sum_{I=1}^{N}\varepsilon^{(I)}(x, z, t)$. Recall that the eigenvalue I is independent of space. It represents the contribution of each mode to the total kinetic energy in the plane of measurement. One can also estimate the dissipation rate of kinetic energy $\langle \varepsilon^{(I)} \rangle$ averaged in the plane:

$$\langle \varepsilon^{(I)} \rangle = \frac{1}{LC}\sum_{l=1}^{L}\sum_{k=1}^{C}\varepsilon^{(I)}(x_l, z_k) \tag{19}$$

It is thus possible to draw a plot similar to the spectrum of eigenvalues; it is the spectrum of dissipation rate of kinetic energy (plot of dissipation rate $\langle \varepsilon^{(I)} \rangle$ associated to mode I versus mode number I). This spectrum will be presented and discussed.

In addition, the strain rate of small scales of turbulence is large and can be expressed as $s'_{ij} \approx u/\lambda$. Recalling Eq. (17) and considering that the P.O.D. coefficient $a_k^{(I)}$ have the dimension of a velocity (m/s), the inverse of a length scale could be associated to the gradients of the eigen-function $\overrightarrow{\Phi^{(I)}}$. This will be analyzed in depth in the discussion.

3.4. Reshaped eigenfunctions

The eigenfunctions are vectors with $2LC$ rows. These vectors can be reshaped to form a (L,C) matrix of local vectors:

$$\overrightarrow{\Phi_k^{(I)}} = \begin{bmatrix} \Phi_{x,k}(x_1, z_1) \\ \Phi_{x,k}(x_2, z_1) \\ \\ \Phi_{x,k}(x_L, z_C) \\ \Phi_{z,k}(x_1, z_1) \\ \Phi_{z,k}(x_2, z_1) \\ \\ \Phi_{z,k}(x_L, z_C) \end{bmatrix} \quad \overrightarrow{\Phi_k^{(I)}} = \begin{bmatrix} \overrightarrow{\Phi_k}(x_1, z_1) & \overrightarrow{\Phi_k}(x_1, z_2) & \overrightarrow{\Phi_k}(x_1, z_C) \\ \overrightarrow{\Phi_k}(x_2, z_1) & \overrightarrow{\Phi_k}(x_2, z_2) & \overrightarrow{\Phi_k}(x_2, z_C) \\ \overrightarrow{\Phi_k}(x_L, z_1) & \overrightarrow{\Phi_k}(x_L, z_2) & \overrightarrow{\Phi_k}(x_L, z_C) \end{bmatrix}$$

$$(20)$$

The reshaped eigenfunction can be plotted in the plane (x,z). It corresponds to a 2D vector field, each vector $\overrightarrow{\Phi_k}(x_i, z_j)$ having a horizontal $\Phi_{x,k}(x_i, z_j)$ and a vertical $\Phi_{z,k}(x_i, z_j)$ component.

3.5. Comments on 2D P.I.V. measurements

The flow field is 3D in the mixing tank. However, the analysis performed with 2D-P.I.V. is limited to a 2D plane of measurement. In terms of mean flow, it is clear that the tangential flow is not measured nor taken into account in the present analysis. Indeed, the goal of the study is 2-folds: one the one hand, it is to extract from the measurements the organized motion induced by the impeller rotation. It was shown in previous studies (Moreau and Liné, 2006, among others) that POD can enable to decompose the organized motion from the instantaneous measurement, without collecting angular phased data. It was also shown by many authors that 2D measurement in a vertical plane enable to extract trailing vortices induced by a Rushton turbine. One the other hand, the goal of this study is to analyze turbulent scales. In terms of turbulence, it was also shown by many authors that the measurement of instantaneous velocity field in a single plane of measurement was

sufficient to estimate the local dissipation rate of turbulent kinetic energy as far as the spatial resolution of the PIV system is high enough. This is related to the isotropy of smallest scales of turbulence coupled to the efficiency of the mixing tank process. Keeping this in mind, we must be aware of the fact that the tangential mean flow is not measured and that associated large scales are not measured too. In terms of POD analysis, the 2D limitation of PIV measurements may affect the largest scales of motion (intermediate modes of POD decomposition).

4. Results

The eigenvalues correspond to the contribution of each mode to the total kinetic energy in the 2D domain of measurement (Section 4.1). Mode 1 is structurally close to the mean (statistical average) velocity field (Section 4.2). When two of the following modes are close to each other in terms of eigenvalues, the energy brought by these modes is the same. Such modes may reveal large scale coherent structures (Sections 4.4 and 4.5). Higher modes may be related to turbulence (Sections 4.5 and 4.6).

4.1. Eigen-value spectrum

The eigen-value spectrum is plotted in Fig. 2. The eigen-values are normalized by the sum of the eigen-values; these normalized eigen-values correspond to the contribution of each mode
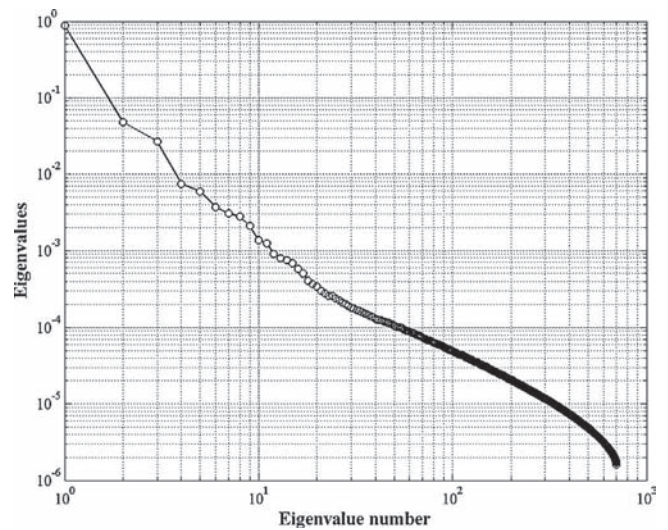
Fig. 2 – Eigen value spectrum.

to the total kinetic energy in the plane of measurement. One can see that the first mode explains more than 80% of the total kinetic energy; it is characteristic of mean flow contribution. One can observe that modes 2 and 3 and modes 4 and 5 are close to each other. They respectively contribute to 3–5% and 0.6–0.8% of the total kinetic energy. The upper modes contribute to lower levels of kinetic energy. One can notice that
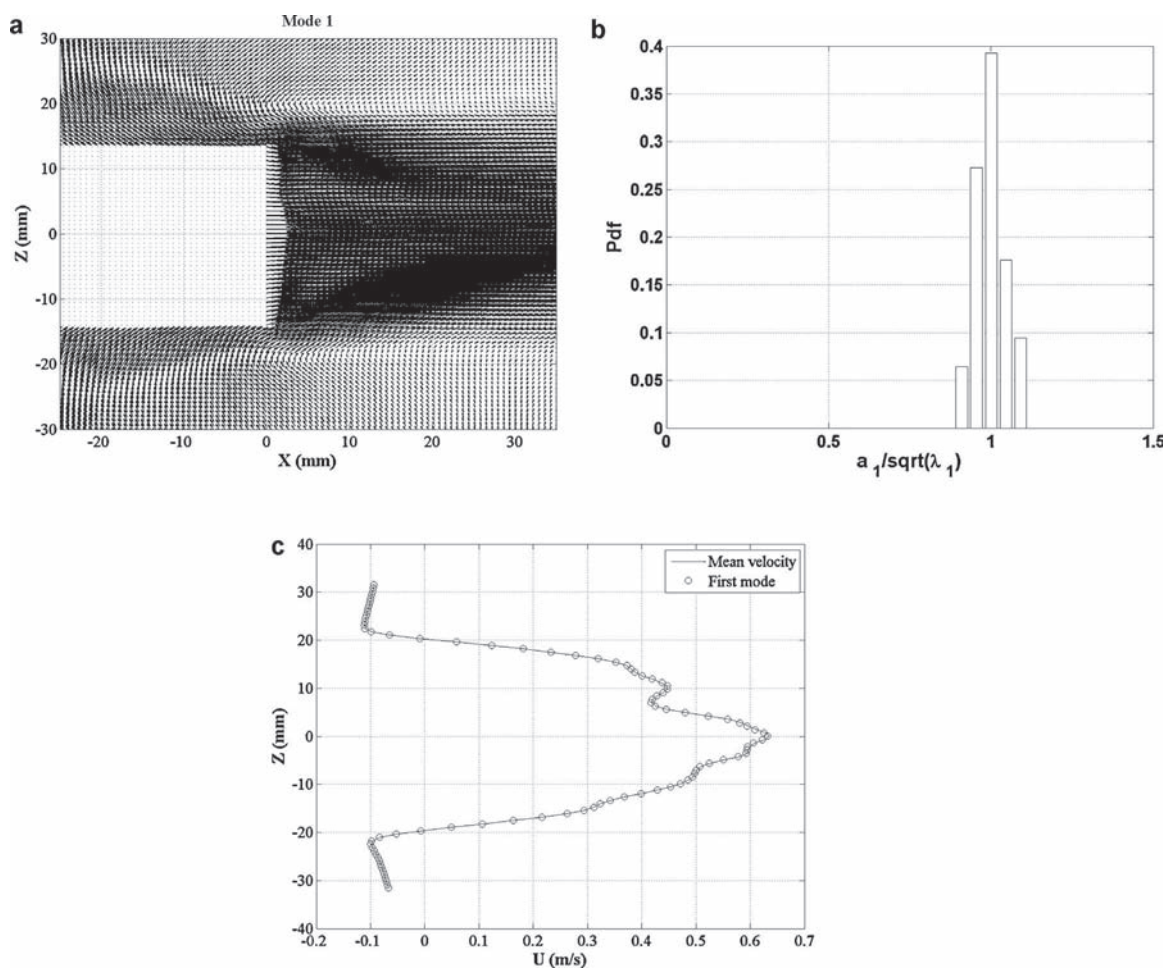
Fig. 3 – First POD mode (a) eigen function, (b) pdf of normalized POD coefficient, and (c) comparison of first mode to mean flow.

upper modes follow a linear trend in log–log plot ($-11/9$); this trend will be explained later in the discussion.

4.2. First mode analysis

The reshaped eigen-function $\overrightarrow{\Phi^{(1)}}(x, z)$ corresponding to mode 1 is plotted in Fig. 3a. It looks like a velocity field but it is not, since the eigen-functions have no dimension. Indeed, the instantaneous velocity field associated to the first mode is given by

$$\overrightarrow{V_k^{(1)}}(x, z, t) = a_k^{(1)}(t)\overrightarrow{\Phi^{(1)}}(x, z) \qquad (21)$$

for each k realization of the velocity. One can plot in Fig. 3b the probability density function of the coefficients $a_k^{(1)}$. The coefficients $a_k^{(1)}$ were normalized by the square root of the first eigen-value $\lambda_R^{(1)}$ expressed in m²/s². The first remark is that the pdf is centered on the unity value; the second remark is the dispersion of the N realizations $a_k^{(1)}$ is weak, meaning that $a_k^{(1)}$ is almost constant. One can thus reconstruct the velocity field associated to the first mode as:

$$\overrightarrow{V_k^{(1)}}(x, z, t) = \sqrt{\lambda_R^{(1)}}\overrightarrow{\Phi^{(1)}}(x, z) \cong cst \quad \forall k \qquad (22)$$

One can compare this velocity field (reconstructed with the first mode) to the statistical average of the instantaneous velocity field, classically defined as:

$$\overrightarrow{V}(x, z, t) = \frac{1}{N}\sum_{k=1}^{N}\overrightarrow{V_k}x(x, z, t) \qquad (23)$$

The vertical profile of the horizontal component of the velocity field reconstructed with the first mode $\overrightarrow{V_k^{(1)}}(x, z, t)$ is compared to the vertical profile of the horizontal component the mean flow $\overrightarrow{V}(x, z, t)$ in Fig. 3c, at a radial position close to the impeller tip. The two profiles are identical. One can thus confirm that the velocity field associated to the first mode is a steady-state field corresponding to the mean flow.

4.3. Organized motion associated to modes 2 and 3

As aforementioned, the eigen-values $\lambda_R^{(2)}$ and $\lambda_R^{(3)}$ have similar orders of magnitude, suggesting that they may correspond to organized motions. This result is expected in mixing with Rushton turbine and may correspond to trailing vortices induced by the impeller blades. The eigen-functions corresponding to mode 2, $\overrightarrow{\Phi^{(2)}}(x, z)$, and 3, $\overrightarrow{\Phi^{(3)}}(x, z)$, are plotted in Fig. 4a and b. These two modes exhibit vortices, almost symmetrical with respect to the plane of the impeller ($z = 0$), suggesting some organization in the structure of these modes. Once again, these plots are not velocity fields. The velocity field associated to the sum of these modes can be written:

$$\overrightarrow{V_k^{(2,3)}}(x, z, t) = \sum_{I=2}^{3}\overrightarrow{V_k^{(I)}}(x, z, t) = a_k^{(2)}(t)\overrightarrow{\Phi^{(2)}}(x, z) + a_k^{(3)}(t)\overrightarrow{\Phi^{(3)}}(x, z) \qquad (24)$$

In order to highlight the link between modes 2 and 3, the k realizations of P.O.D. coefficients $a_k^{(2)}$ were plotted versus the k realizations of P.O.D. coefficients $a_k^{(3)}$ in Fig. 5a. A 2D projection
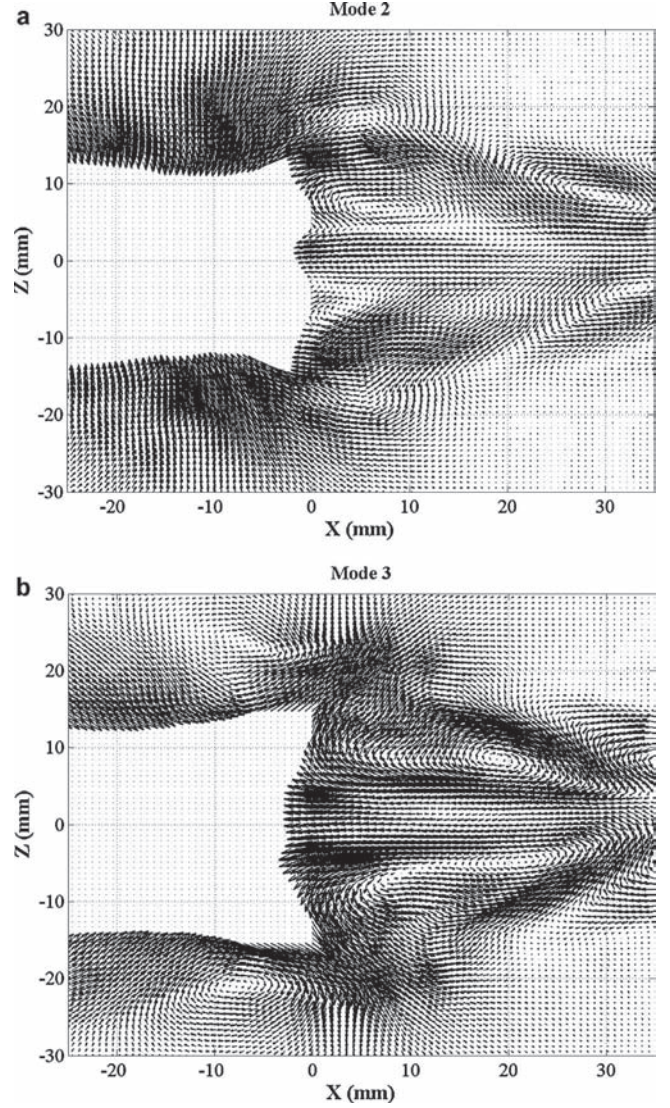

Fig. 4 – POD eigen functions of (a) mode 2 and (b) mode 3.

of the phase portrait in the ($a_k^{(2)}$, $a_k^{(3)}$) plane is thus obtained. The set of data show an organized shape; for sake of simplicity, it will be considered as an ellipse. The coefficients can thus be related by the expression:

$$\frac{a_k^{(2)2}}{2\lambda_R^{(2)}} + \frac{a_k^{(3)2}}{2\lambda_R^{(3)}} = 1 \qquad (25)$$

where the eigen-values are expressed in m²/s². The periodic nature of these coherent structures associated with modes 2 and 3 could be expressed as sinusoidal variations $a^{(2)}(\varphi_k)$ and $a^{(3)}(\varphi_k)$ as shown in previous papers (Ducci et al., 2007; Doulgerakis et al., 2011; Gabelle et al., 2013):

$$a^{(2)}(\varphi_k) = \sqrt{2\lambda_R^{(2)}}\cos(\varphi_k) \quad \text{and} \quad a^{(3)}(\varphi_k) = \sqrt{2\lambda_R^{(3)}}\sin(\varphi_k) \qquad (26)$$

where φ_k is the phase angle. The parameters $a^{(2)}(\varphi_k)$ and $a^{(3)}(\varphi_k)$ have the dimension of velocities (m/s). It is thus possible to reconstruct the temporal evolution of the organized motion associated to modes 2 and 3:

$$\overrightarrow{V_k^{(2,3)}}(x, z, t) = \sqrt{2\lambda_R^{(2)}}\cos(\varphi_k)\overrightarrow{\Phi^{(2)}}(x, z) + \sqrt{2\lambda_R^{(3)}}\sin(\varphi_k)\overrightarrow{\Phi^{(3)}}(x, z) \qquad (27)$$
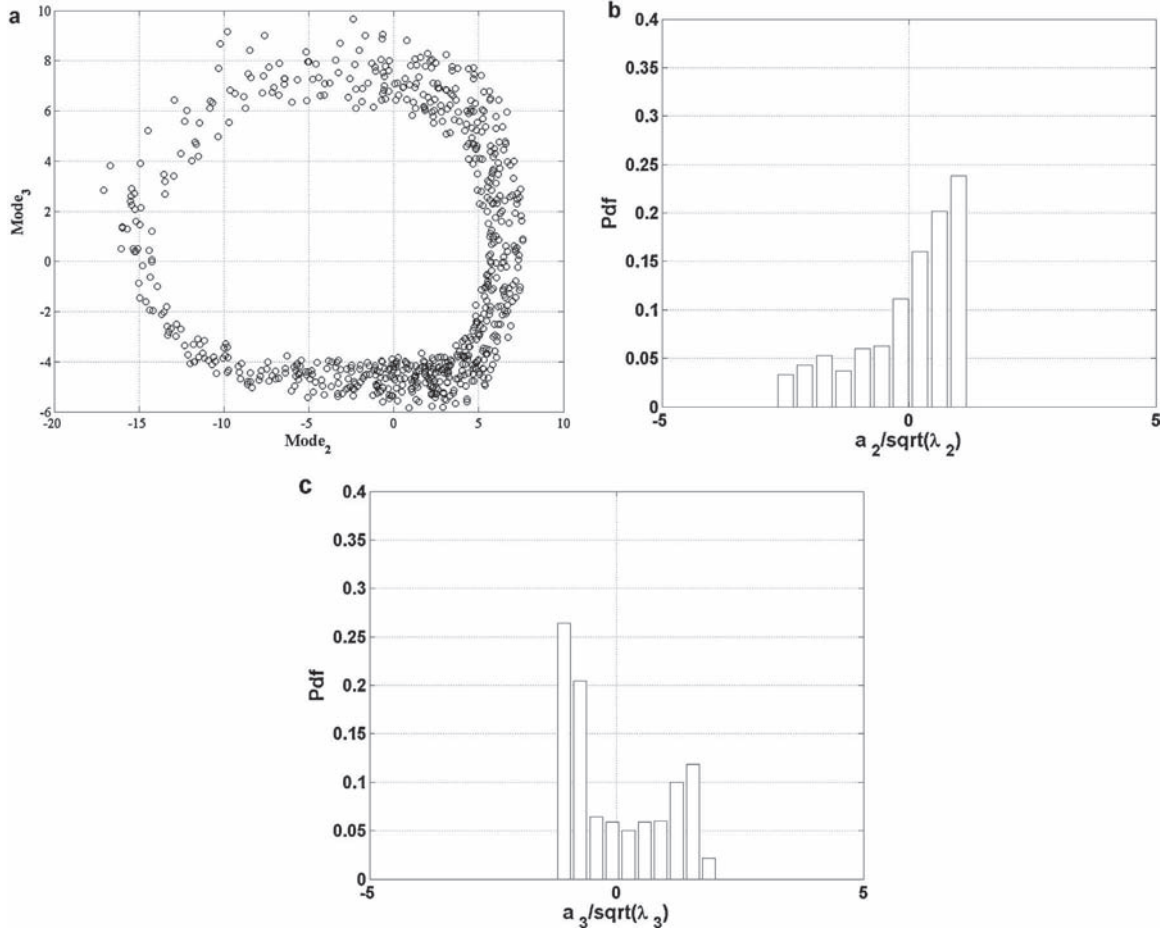
Fig. 5 – Modes 2 and 3: (a) portrait of phase, (b) pdf of normalized POD coefficient of mode 2, and (c) pdf of normalized POD coefficient of mode 3.

One can plot in Fig. 5c and d the probability density functions of the normalized coefficients $a_k^{(2)}/\sqrt{\lambda_R^{(2)}}$ and $a_k^{(3)}/\sqrt{\lambda_R^{(3)}}$. The distributions are centered on the origin and their shape can be related to sinusoidal distributions, as expected from the previous analysis.

4.4. Organized motion associated to modes 4 and 5

As aforementioned, the eigen-values $\lambda_R^{(4)}$ and $\lambda_R^{(5)}$ have also similar orders of magnitude and may thus contribute to organized motions. The eigen-functions corresponding to mode 4, $\overrightarrow{\Phi^{(4)}}(x, z)$, and mode 5, $\overrightarrow{\Phi^{(5)}}(x, z)$, are plotted in Fig. 6a and b. Compared to modes 2 and 3, modes 4 and 5 show again vortical structures but the length-scales seem to be roughly half the length-scales of modes 2 and 3. Similarly to the previous analysis of modes 2 and 3, the k realizations of $a_k^{(4)}$ were plotted versus the k realizations of $a_k^{(5)}$ in Fig. 7a and the probability density functions of the coefficients $a_k^{(4)}/\sqrt{\lambda_R^{(4)}}$ and $a_k^{(5)}/\sqrt{\lambda_R^{(5)}}$ were plotted in Fig. 7b and c, the eigen values being expressed in m^2/s^2. Fig. 7a exhibits a strong relation between modes 4 and 5 whereas the pdf distributions reveal noisy sinusoidal distributions. In order to go in deeper depth, the modes 4 and 5 have been plotted versus modes 2 and 3 in Fig. 8a–d. 2D projections of the phase portrait are thus plotted for different bases. The organized structures revealed by these plots exhibit two lobes (contrary to the previous portrait of phases

plotted in Fig. 5, with only one lobe) and can be analyzed as follows:

- the relation between mode 2 and mode 4 (Fig. 8a) corresponds roughly to a plot of $\sin(2\varphi_k - (\pi/2))$ versus $\cos(\varphi_k)$, that is $-\cos(2\varphi_k)$ versus $\cos(\varphi_k)$;
- the relation between mode 2 and mode 5 (Fig. 8b) corresponds roughly to a plot of $\sin(2\varphi_k)$ versus $\cos(\varphi_k)$;
- the relation between mode 3 and mode 4 (Fig. 8c) corresponds roughly to a plot of $\sin(2\varphi_k + (\pi/2))$ versus $\cos(\varphi_k)$, that is $\cos(2\varphi_k)$ versus $\cos(\varphi_k)$;
- the relation between mode 2 and mode 5 (Fig. 8b) corresponds again to a plot of $\sin(2\varphi_k)$ versus $\cos(\varphi_k)$.

Modes 4 and 5 follow thus a sinusoidal trend, with a period which is half the period of modes 2 and 3. It is thus possible to reconstruct the temporal evolution of the organized motion associated to modes 4 and 5:

$$\overrightarrow{V_k^{(4,5)}}(x, z, t) = -\sqrt{2\lambda_R^{(4)}}\cos(2\varphi_k)\overrightarrow{\Phi^{(4)}}(x, z)$$

$$+ \sqrt{2\lambda_R^{(5)}}\sin(2\varphi_k)\overrightarrow{\Phi^{(5)}}(x, z) \qquad (28)$$

The structures revealed by modes 2 to 5 can be compared to vortex shedding behind bluff bodies that have been investigated by many workers since the pioneering paper of Roshko (1955). Similar Lissajous figures were obtained in their works.
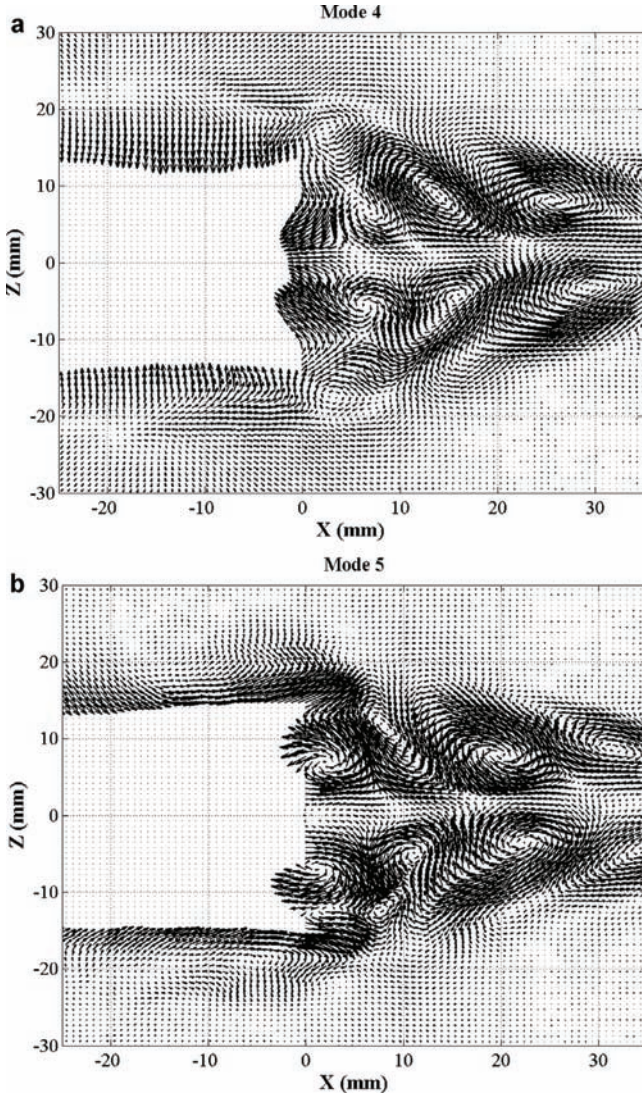
Fig. 6 – POD eigen functions of (a) mode 4 and (b) mode 5.

4.5. Turbulent motion

Following the decomposition method, a reconstruction of the turbulence is based on all the modes higher than 6:

$$\overrightarrow{V_k^{(\text{turb})}}(x, z, t) = \sum_{I=6}^{N} \overrightarrow{V_k^{(I)}}(x, z, t) = \sum_{I=6}^{N} a_k^{(I)}(t) \overrightarrow{\Phi^{(I)}}(x, z) \quad (29)$$

The probability density function of horizontal (u_k') component of the turbulent velocity vector given by Eq. (29) is plotted in Fig. 9a, in a point located in the jet of the impeller. The pdf are significantly different from the previous ones; a Gaussian function based on the mean and rms values of this distribution is plotted and fits perfectly the data.

4.6. Kinetic energy dissipation rate spectrum

As afore-mentioned, one can derive the Ith component of the rate of viscous dissipation of kinetic energy averaged in the plane, $\langle \varepsilon^{(I)} \rangle$, expressed by Eq. (19). It is thus possible to plot the distribution of rate of viscous dissipation associated to each I mode versus the mode number, similarly to the eigen-value spectrum (Fig. 2). This kinetic energy dissipation rate spectrum

is plotted in Fig. 9b. One can notice that upper modes follow a linear trend in log–log plot (−5/9); this trend is related to the −11/9 slope of the eigen-value spectrum plotted in Fig. 2, as it will be explained later in the discussion.

5. Discussion

5.1. Eigenvalue spectrum

The eigen-value spectrum exhibits a −11/9 slope in log–log plot of $\lambda^{(I)}$ versus the eigen-value number I. This result was explained by Knight and Sirovich (1990) arguing that it is a characteristic of inertial range of turbulence. As exposed by these authors, in turbulent flows, the turbulent kinetic energy (*tke*) can be related to the energy density spectrum of velocity $E_V(K)$, per vector wave number K, as:

$$tke = \frac{1}{\vartheta} \iiint u^2 \, dv = \iiint E_V(K) \, dK \quad (30)$$

Clearly, the dimension of the energy density spectrum of velocity $E_V(K)$ is $\dim[E_V] = l^5/t^2$ or l^2/t^2 times l^3. It corresponds to a kinetic energy in a volume. In the inertial range of turbulence, assuming turbulence isotropy, one can write the energy density spectrum of velocity E_V per vector wave number in terms of the energy density spectrum of velocity $E_S(\kappa)$ per scalar wave number κ: $E_V = E_S(\kappa)/4\pi\kappa^2$. The trend of the energy density spectrum of velocity $E_S(\kappa)$ per scalar wave number is well known $E_S(\kappa) \propto \varepsilon^{2/3} \kappa^{-5/3}$. One can thus derive the energy density spectrum of velocity $E_V(\kappa)$ per vector wave number as $E_V \propto \varepsilon^{2/3} \kappa^{-11/3}$.

Knight and Sirovich (1990) considered then the POD analysis. As aforementioned in Section 3.1, the eigenvalue $\lambda^{(I)}$ is expressed in m^5/s^2 in a full 3D analysis, similarly to the energy density spectrum of velocity E_V per vector wave number. Thus, Knight and Sirovich (1990) considered that each eigen value is a generalization of the energy density spectrum of velocity E_V, carrying the same physical dimensions. It follows $\lambda^{(I)} \propto \kappa^{-11/3}$. In addition, Knight and Sirovich (1990) stipulated that the wave number may be related to the eigenvalue number as $\kappa \propto I^{1/3}$. Thus, they obtained the −11/9 trend $\lambda^{(I)} \propto I^{-11/9}$. This trend is observed in our data processing (Fig. 2). This result is surprising at first appearance, since the Reynolds number of the flow in the tank is low (it is equal to 530), corresponding to the "transition" region of turbulence. It is known that local isotropy only exist if the local Reynolds number is large enough. The first argument is that the global Reynolds number is low but the hydrodynamics is heterogeneous in the tank. The level of turbulence is higher close to the impeller (where the data where acquired) than far from it. Secondly, Knight and Sirovich have shown that an inertial range can exist at very modest Reynolds numbers. Such −11/9 trend was also observed in the same mixing tank with another shear thinning fluid (with yield stress, Carbopol, Gabelle et al., 2013) but this trend was limited to the higher Reynolds number.

One must also highlight that the −11/9 trend corresponds to modes larger than 20. This relatively large value can be explained by the limitation of 2D measurement of a 3D velocity field. As aforementioned, the velocity component normal to the 2D plane of measurement is not measured. In addition, the choice of Zetag fluid was dictated in order to limit the turbulence level close to the impeller; it was thus possible to measure almost all the turbulent scales. Therefore, the
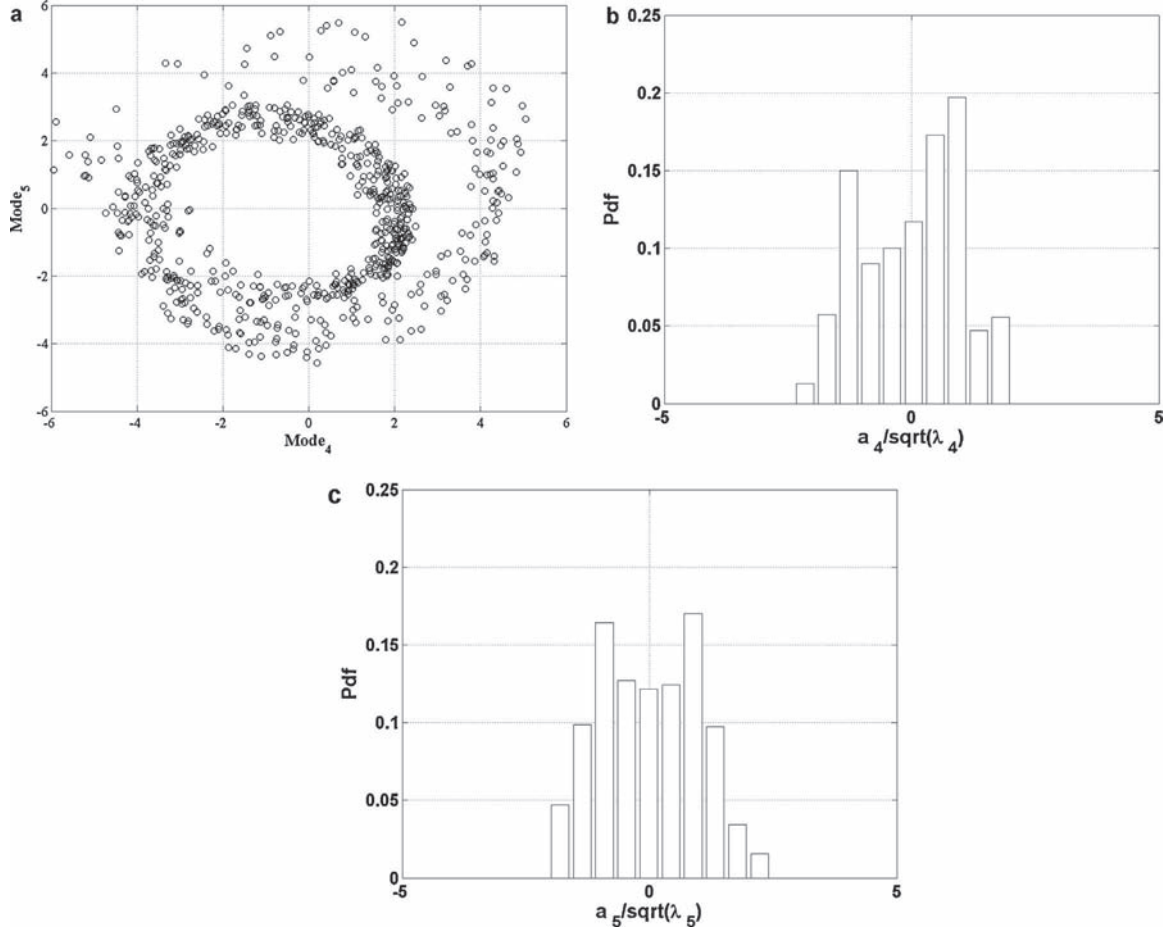
Fig. 7 – Modes 4 and 5: (a) portrait of phase, (b) pdf of normalized POD coefficient of mode 4, and (c) pdf of normalized POD coefficient of mode 5.

main issue of this work is to exhibit the $-11/9$ trend of the eigen-value spectrum for large values of modes, corresponding to turbulent motion.

5.2. Dissipation rate spectrum

One can extend the development proposed by Knight and Sirovich (1990) to the analysis of the spectrum of kinetic energy dissipation rate, plotted in Fig. 9b. This spectrum exhibits a linear trend in log–log plot with a slope $-5/9$. This result can be explained as follows. The spectrum of the dissipation in scalar wave number can be expressed as:

$$\varepsilon = \int D(\kappa)\, d\kappa \tag{31}$$

The dissipation density spectrum can be related to the energy density spectrum by $D(\kappa) \approx \kappa^2 E(\kappa) \propto \kappa^{-5/3}$. Considering once more that the scalar wave number is related to the eigen-value number by $\kappa \propto I^{1/3}$, we obtain the trend $-5/9$ that is observed in the plot of $\langle \varepsilon^{(I)} \rangle$, normalized by the total dissipation rate (summation for all modes). This total dissipation rate is equal to 0.42 W/kg, almost twice the volume averaged value of the dissipation rate of kinetic energy $\langle \varepsilon \rangle$ which is equal to 0.2 W/kg.

Here again, the $-5/9$ trend corresponds to modes larger than 20. However, the main issue of this work is to explain the $-5/9$ trend of the dissipation spectrum for large values of modes, corresponding to turbulent motion.

5.3. Wave number associated to the mode I

The last question is related to the assumption stating that $\kappa \propto I^{1/3}$. Recall first that the reconstruction process is given by Eq. (1). The dimension of the coefficient $a_k^{(I)}$ is l/t whereas the eigen-function $\overrightarrow{\Phi^{(I)}}(x, z)$ has no dimension. In addition, the coefficient $a_k^{(I)}$ is constant in the domain and only depends on the time whereas the eigen-function $\overrightarrow{\Phi^{(I)}}(x, z)$ is constant with time but it varies in the spatial coordinates (x,z). Consequently, any length-scale associated to the Ith mode can only be related to the eigen-function $\overrightarrow{\Phi^{(I)}}(x, z)$ and cannot be related to the P.O.D. coefficient which is constant for each mode in the plane. It is thus foreseeable that the wave number associated to each I mode depends on the eigen-function $\overrightarrow{\Phi^{(I)}}(x, z)$ and/or on its gradients. If (V_x, V_z) are the horizontal and vertical components of the velocity vector $\overrightarrow{V}$, and $[\Phi_x^{(I)}(x, z), \Phi_z^{(I)}(x, z)]$ are the horizontal and vertical components of the eigen-function $\overrightarrow{\Phi^{(I)}}(x, z)$, one can express the cross-correlation function A_{xx} of the horizontal velocity V_x between (x,z) and $(x+L,z)$ as:

$$A_{xx}(L) = \overline{V_x(x, z) V_x(x + L, z)} = \frac{1}{N} \sum_{k=1}^{N} V_{x,k}(x, z) V_{x,k}(x + L, z) \tag{32}$$
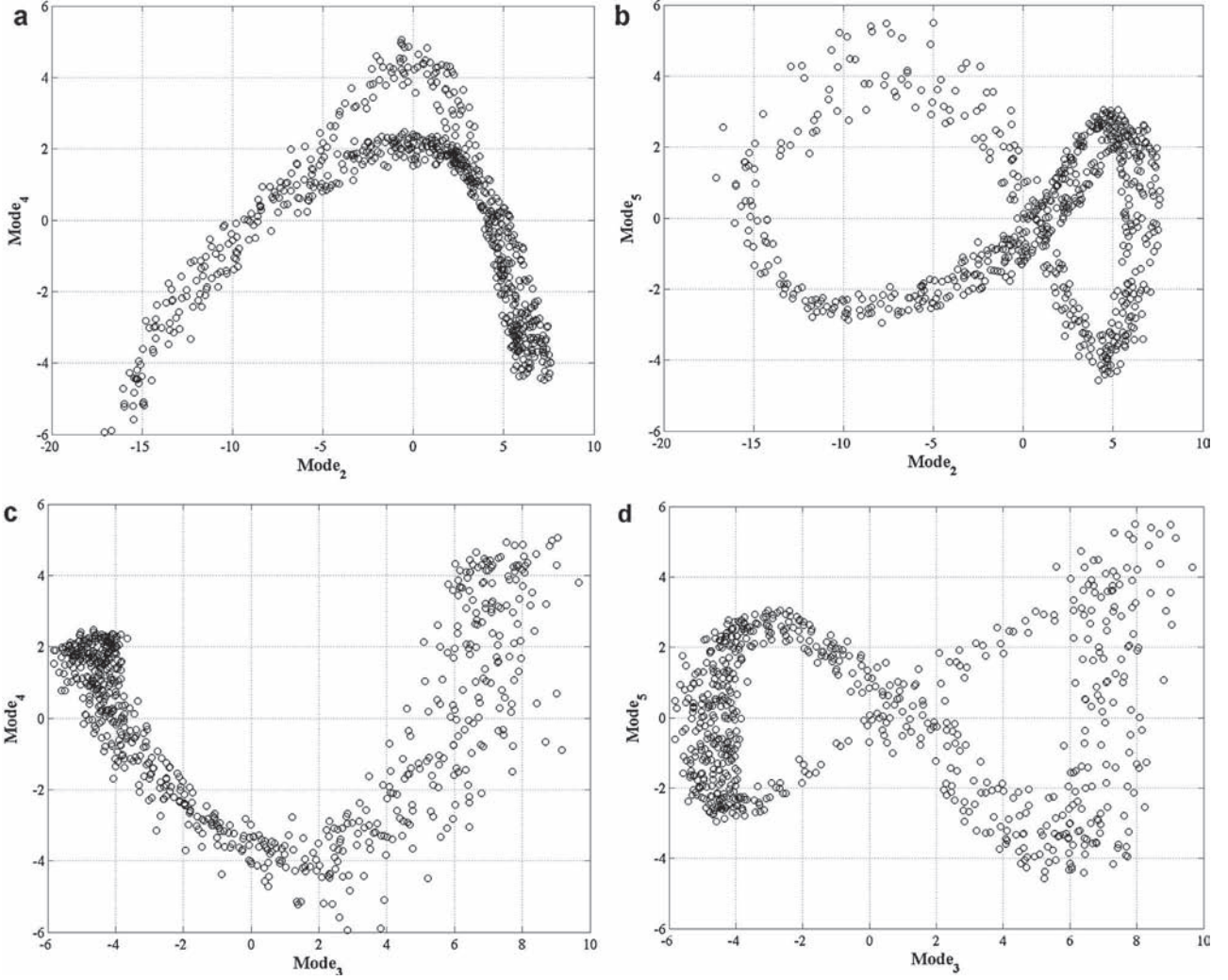
Fig. 8 – Portrait of phase: (a) base 2-4, (b) base 2-5, (c) base 3-4, and (d) base 3-5.

After derivation, based on the reconstruction process and on Eq. (14), one obtains:

$$A_{xx}(L) = \overline{V_x(x, z)V_x(x + L, z)} = \sum_{I=1}^{N} \lambda_R^{(I)} \Phi_x^{(I)}(x, z)\Phi_x^{(I)}(x + L, z) \qquad (33)$$

In other words, for each mode I, one can define a cross-correlation function $A_{xx}^{(I)}$ in terms of $A_{xx}^{(I)}(L) = \lambda^{(I)}\Phi_x^{(I)}(x, z)\Phi_x^{(I)}(x + L, z)$ or in non-dimensional form:

$$R_{xx}^{(I)}(L) = \frac{A_{xx}^{(I)}(L)}{\lambda_R^{(I)}} = \Phi_x^{(I)}(x, z)\Phi_x^{(I)}(x + L, z) \qquad (34)$$

A Taylor development at the origin gives

$$R_{xx}^{(I)}(L) = 1 - \frac{x^2}{2}\left[\frac{\partial\Phi_x^{(I)}}{\partial x}\right]^2 = 1 - \kappa_x^{(I)2}x^2 \qquad (35)$$

Thus, a wave number can easily be related to the spatial gradient of the eigen-function $\overrightarrow{\Phi^{(I)}}(x, z)$.

Indeed, the kinetic energy dissipation rate associated to each mode I was expressed by Eq. (18). Dimensionally, one can consider a wave number associated to each I mode and defined by:

$$\kappa^{(I)}(x_l, z_k) = \sqrt{\sum_{i=1}^{3}\sum_{j=1}^{3}\left(\frac{\partial\Phi_i^{(I)}(x_l, z_k)}{\partial x_j} + \frac{\partial\Phi_j^{(I)}(x_l, z_k)}{\partial x_i}\right)^2} \qquad (36)$$

This wave numbers can easily be derived from the eigen-function gradients. In fact this wave number varies in the plane of measurement. Since the eigenvalue is an average of the kinetic energy in the plane of measurement associated to mode I and $\langle\varepsilon^{(I)}\rangle$ is also averaged in the plane of measurement, one can estimate an average of the wave number in the plane $\langle\kappa^{(I)}\rangle$ similarly to Eq. (19).

This averaged wave number $\langle\kappa^{(I)}\rangle$ is normalized by the wave number of the first mode and plotted versus the eigenvalue number I in Fig. 10. The curve $I \propto \langle\kappa^{(I)}\rangle^3$ is also plotted. The normalized averaged wave numbers issued from the eigen-functions gradients behaves as the wave number power 1/3, as stipulated by Knight and Sirovich. The definition of the wave number associated to the Ith mode, $\kappa^{(I)}$, is a generalization of this simplified development given by Eq. (35). Further analysis should be done on the pdf of gradients of eigen functions in the plane of measurement for each I mode to better understand the physical meaning of this scale.
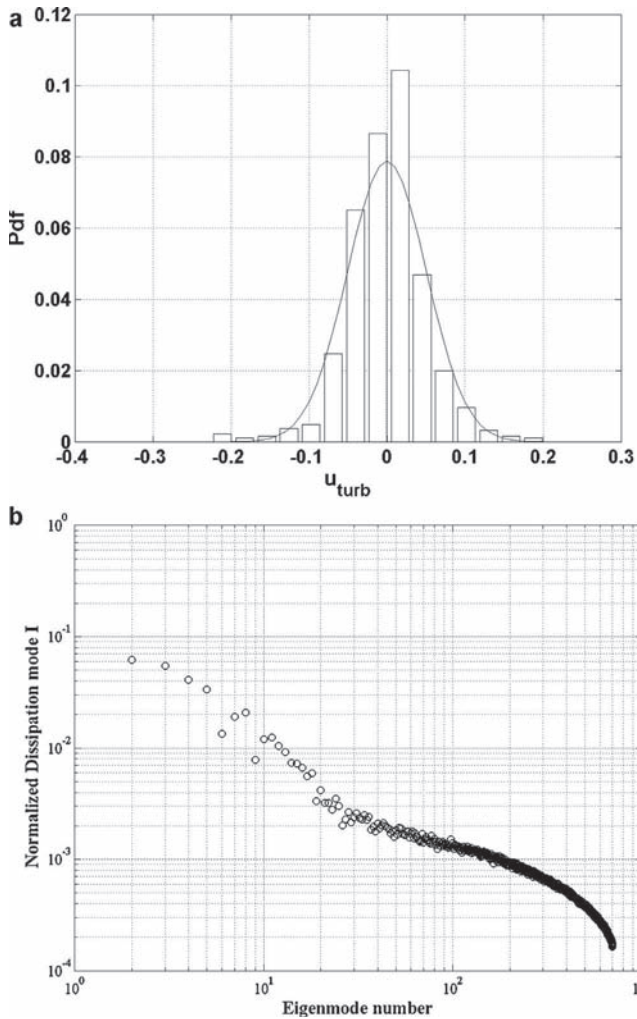
Fig. 9 – Turbulence (a) pdf of turbulent velocity fluctuations and (b) spectrum of dissipation rate of kinetic energy.
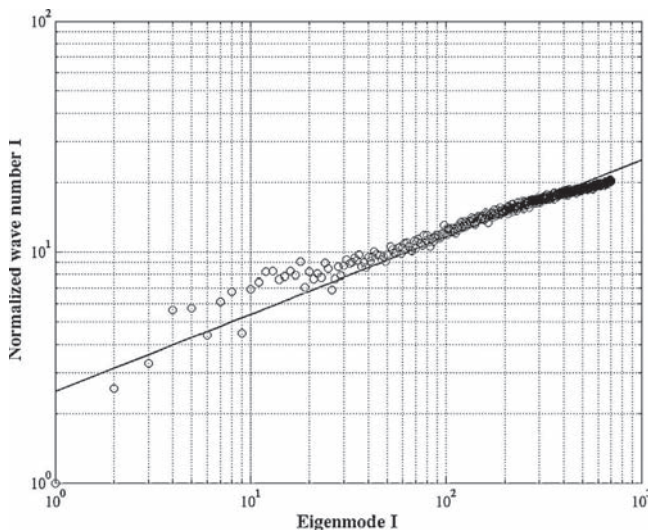

Fig. 10 – Wave number versus eigen mode number.

6. Conclusion

P.O.D. technique was applied to 2D P.I.V. data. Each instantaneous velocity field can be expanded in a series of P.O.D. modes. The first mode is associated to mean flow. The following pairs of modes are associated to trailing vortices. The higher modes are related to turbulence. The −11/9 trend of the eigen-value spectrum is verified. The spectrum of dissipation rate of kinetic energy is plotted and the −5/9 trend is shown and explained. Length scales associated to each mode are determined and plotted versus mode number. The power 3 trend is shown. The goal of this paper was to show the different trends (−11/9 trend of the eigen-value spectrum, −5/9 for the spectrum of dissipation rate of kinetic energy, and 3 for the length scales associated to each mode) corresponding to turbulent motions. Clearly these trends are limited to modes larger than 20. The analysis of the full 3D flow should be completed to improve the understanding and the quality of both measurement and processing of the P.O.D. modes lower than 20.

References

Berkooz, G., Holmes, P., Lumley, J.L., 1993. Proper orthogonal decomposition in the analysis of turbulent flows. Annu. Rev. Fluid Mech. 25, 539–575.

De Angelis, E., Casciola, C.M., L'vov, V.S., Piva, R., Procaccia, I., 2003. Drag reduction by polymers in turbulent channel flows: energy redistribution between invariant empirical modes. Phys. Rev. E 67, 050612.

Ducci, A., Doulgerakis, Z., Yianneskis, M., 2007. Decomposition of flow structures in stirred reactors and implications for mixing enhancement. Ind. Eng. Chem. Res. 47, 3664–3676.

Doulgerakis, Z., 2010. Large Scale Vortex and Strain Dynamics in Mixing Vessels and Implications for Macro-mixing Enhancement. King's College, University of London, UK (PhD).

Doulgerakis, Z., Yianneskis, M., Ducci, A., 2011. On the manifestation and nature of macroinstabilities in stirred vessels. AIChE J. 57, 2941–2954.

Escudier, M.P., Smith, S.E., 2001. Fully developed turbulent flow of Newtonian liquids through a square duct. Proc. R. Soc. London, Ser. A 457, 911.

Gabelle, J.-C., Morchain, J., Anne-Archard, D., Augier, F., Liné, A., 2013. Experimental determination of the shear rate in a stirred tank with non-newtonian fluid. AIChE J. 59 (6), 2251–2266.

Hoisiadas, K.D., Beris, A.N., Handler, R.A., 2005. Viscoelastic effects on higher order statistics and on coherent structures in turbulent channel flow. Phys. Fluids 17, 035106.

Knight, B., Sirovich, L., 1990. Kolmogorov inertial range for inhomogeneous turbulent flows. Phys. Rev. Lett. 65, 1356–1359.

Moreau, J., Liné, A., 2006. Proper orthogonal decomposition for the study of hydrodynamics in a mixing tank. AIChE J. 52, 2651–2655.

Oudheusden, B.W., van Scarano, F., Hinsberg, N.P., van Watt, D.W., 2005. Phase-resolved characterization of vortex shedding in the near wake of a square-section cylinder at incidence. Exp. Fluids 39, 86–98.

Roshko, A., 1955. On the wake and drag of bluff bodies. J. Aerosp. Sci. Technol. 22, 124–132.

Sirovich, L., 1987. Turbulence and the dynamics of coherent structures. Q. Appl. Math. 45, 561–590.

Tabib, M.V., Joshi, J.B., 2008. Analysis of dominant flow structures and their flow dynamics in chemical process equipment using snapshot proper orthogonal decomposition technique. Chem. Eng. Sci. 63, 3695–3715.